Interfacial Tension Hysteresis of Eutectic Gallium-Indium

*Keith D. Hillaire, Praneshnandan Nithyanandam, Minyung Song, Sahar Rashid Nadimi, Abolfazl Kiani, Michael D. Dickey, and Karen E. Daniels**

When in a pristine state, gallium and its alloys have the largest interfacial tensions of any liquid at room temperature. Nonetheless, applying as little as 0.8 V of electric potential across eutectic gallium indium (EGaIn) placed within aqueous sodium hydroxide (NaOH, or other electrolyte) solution will cause the metal to behave as if its interfacial tension is near zero. The mechanism behind this phenomenon has remained poorly understood because NaOH dissolves the oxide species, making it difficult to directly measure the concentration, thickness, or chemical composition of the film that forms at the interface. In addition, the oxide layers formed are atomically-thin. Here, it presents a suite of techniques that allow to simultaneously measure both electrical and interfacial properties as a function of applied electric potential, allowing for new insights into the mechanisms, which cause the dramatic decrease in interfacial tension. A key discovery from this work is that the interfacial tension displays hysteresis while lowering the applied potential. It combines these observations with electrochemical impedance spectroscopy to evaluate how these changes in interfacial tension arise from chemical, electrical, and mechanical changes on the interface, and close with ideas for how to build a free energy model to predict these changes from first principles.

K. D. Hillaire, K. E. Daniels
Dept. of Physics
NC State University
Raleigh, NC 27695, USA
E-mail: kdaniel@ncsu.edu
P. Nithyanandam, M. Song, S. R. Nadimi, A. Kiani, M. D. Dickey
Dept. of Chemical and Biomolecular Engineering
NC State University
Raleigh, NC 27695, USA
S. R. Nadimi
Physical Science Department
Bakersfield College
Bakersfield, CA 93305, USA
A. Kiani
Department of Chemistry and Biochemistry
California State University
Bakersfield, CA 93311, USA

1. Introduction

A suite of desirable properties — electrochemically tunable interfacial tension down to negligible values, high thermal, and electrical conductivity, low viscosity, non-toxicity — make gallium-based liquid metals particularly promising for use in soft and reconfigurable devices,[1–7] including pumps,[8] actuators,[9] valves,[10] and RF devices[11] by injecting the liquid metals into microfluidic channels.[12–16] Of particular interest is the room-temperature liquid eutectic gallium indium (EGaIn). The reversible and highly-effective electrochemical tunability of its interfacial tension is remarkably different from conventional, surfactant-based approaches that only modestly decrease the interfacial tension (by $\approx 20 - 50$ mNm^{-1})[17] and are typically difficult to remove.[18] The electrochemical methods further surpass the effectiveness of electrocapillarity,[2,8,10,19–21] whereby an applied electric potential modifies the electric double layer on the surface of the metal in an electrolyte and thereby lowers the interfacial tension without changing the chemistry.[6] A schematic of the electrochemical method is shown in **Figure 1**. When a voltage is applied to a droplet and then removed, the droplet flattens and then returns to its original shape.

Utilizing electrochemical oxidation of the surface of EGaIn within an electrolyte provides rapid and reversible control of interfacial tension over an enormous range (≈ 500 mNm^{-1} at 0 V to nearly 0 mNm^{-1} at ≈ 0.8 V),[3,22] well beyond what is achievable by conventional methods for controlling surface effects. The dramatic effects of this tunability generate surprising fluid behaviors through exploiting classic fluid instabilities under applied electric potentials: destabilizing droplets into fractal spreading patterns,[5,22] or stabilizing thin liquid streams.[23,24]

While Figure 1 illustrates the interfacial properties reversing after a complete voltage cycle, there is hysteresis present during intermediate steps. By examining the detailed dynamics under forward and reverse voltage sweeps, we can use these intermediate steps to test hypotheses about the specific electrochemical processes, which underlie the observations. The observed decrease in interfacial tension has been speculated to arise from surfactant-like oxide(s) forming by electrochemical reactions, with the observed drop in interfacial tension coinciding with the onset of oxide formation,[3,22] as has also been observed
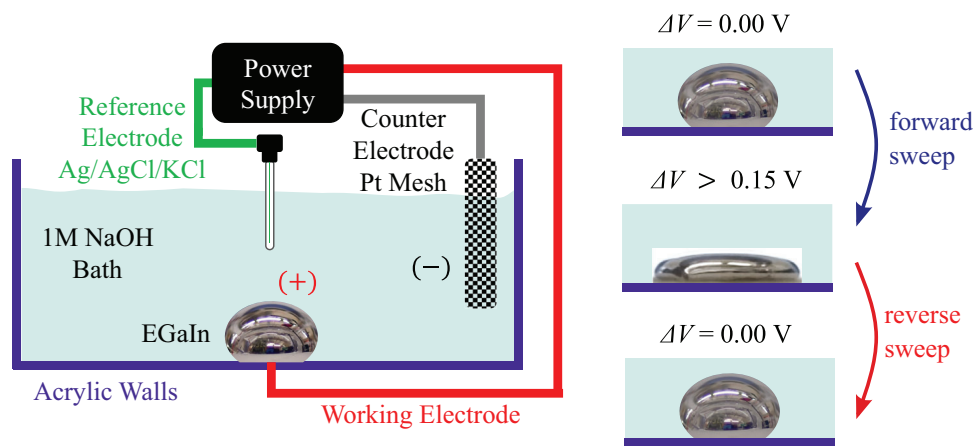
Figure 1. a) A 100 µL sessile droplet of EGaIn is in placed in a 1M NaOH solution (light blue background), with the three-electrode configuration shown schematically. At open circuit potential ($\Delta V = 0$ V), the liquid metal has high interfacial tension, but flattens above $\Delta V \approx 0.15$ V due to a dramatic drop in interfacial tension. When the applied voltage is returned to $\Delta V = 0$ V, the higher interfacial tension returns and the droplet retracts to its original shape.

that the interfacial tension of liquid aluminum decreases with the oxygen content of its environment.[25] Further studies suggested that the oxide species may additionally create compressive forces at larger applied voltages,[22] but the precise mechanisms have remained poorly understood. In this paper, we aim to critically evaluate the possible chemical, electrical, and interfacial mechanisms that lead to the dependence of the interfacial tension on applied electric potential by comparing impedance spectroscopy and interfacial tension measurements, and highlight future avenues for study.

2. Results and Discussion

2.1. Cyclic Voltammetry on Sessile Droplets

Using a sessile (stationary) droplet of 100 µL of EGaIn (Ga 75.5%, In 24.5%) in a NaOH solution, as shown in Figure 1, we simultaneously measure (1) the interfacial tension γ from image analysis of the droplet shape during anodic oxidation and (2) the electrical current I using a potentiostat with a Ag/ AgCl/ KCl reference electrode to maintain an applied electric potential ΔV. Each experimental run consists of a cycling ΔV between the open circuit potential V_{OC}, a maximum applied potential V_{max}, and back to V_{OC} at a quasistatic rate of 10 mVs^{-1}. The potentiostat records the current I passing between the working electrode and the counter electrode; to determine the current density $J = I/a$ considered the area a of the droplet's upper, exposed surface. The surface area was measured from the detected edge of the droplet, integrated under the assumption of a radially symmetric droplet. Details of these methods are given in Section 4.

We image the droplet from the side; by synchronizing this video with step controls on the DC power supply, we measure $\gamma(\Delta V)$. As shown in **Figure 2**, we observe four clear transitions to which we assign names. The first occurs at the sharp rise in current density J, which we associate to the open circuit potential V_{OC}, located at -1.53 V measured with respect to the Ag/AgCl/KCl electrode. We assign this value to be $\Delta V = 0$, and all voltages in this paper are measured relative to it. The second transition occurs at the passivating voltage $V_P \approx (0.10 \pm 0.01)$ V,

at which the current J sharply drops to a plateau two orders of magnitude lower. The third transition, at $V_{SQ} \approx (0.15 \pm 0.01)$ V, is associated with the start of an approximately quadratic shape with $\Delta\gamma(\Delta V) \propto \Delta V^2$, followed by the fourth transition to an approximately linear trend above $V_L \approx (0.27 \pm 0.01)$ V. Within this
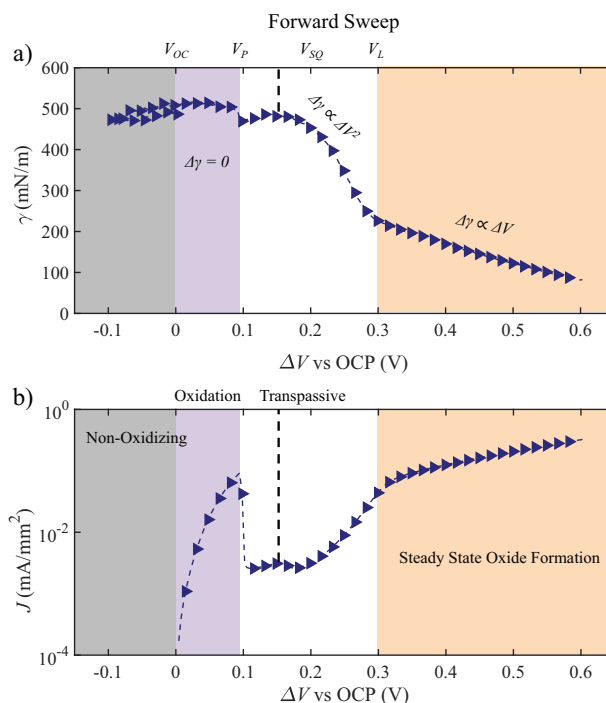

Figure 2. Typical forward voltage sweep experiment (10 mVs^{-1} sweep rate), with voltage shown relative to the open circuit potential V_{OC} and ΔV_{max} = 0.6 V. Voltage-dependence of the (a) interfacial tension γ and (b) current density J are shown in parallel, with the four electrochemical regimes described in the text marked as colored bands: non-oxidizing, oxidation, transpassive, and steady state oxide formation. The dashed line corresponds to the transition between diffusive and inductive transpassive behavior. A summary of the voltage variables and their subscripts appears in **Table 1**.

Table 1. Table of voltage abbreviations.

Symbol	Definition
ΔV	difference from open circuit voltage
V_{OC}	open circuit voltage ($\Delta V = 0$)
V_P	onset voltage of passivation
V_{SQ}	onset voltage of quadratic decrease in tension
V_L	onset voltage of linear decrease in tension

forward sweep, we observe that the interfacial tension is approximately constant ($\gamma_0 \approx (500 \pm 15)$ mNm⁻¹) over the range $V_{OC} < \Delta V < V_{SQ}$, after which a two-stage decrease occurs. The transition at V_P is further demarcated by the observation that for experiments in which the same NaOH solution was reused multiple times, an additional dip in $\gamma(\Delta V)$ was observed at this point.

For the reverse voltage sweep (from ΔV_{max} back to zero), these transitions are modified. As shown in **Figure 3**, we observe hysteresis at intermediate voltages. We identify a voltage $V_{jump} \approx (0.06 \pm 0.01)$ V above which the interfacial tension γ and current density J are history-dependent. This voltage is below the passivating transition at V_P observed during the forward sweep, and is characterized by sharp increases in both γ and J as the voltage

is lowered. Once the system returns below V_{jump}, the interfacial tension returns to $\gamma_0 \approx (500 \pm 15)$ mNm⁻¹.

Within the hysteretic regime, $\gamma(\Delta V)$ no longer follows the quadratic shape observed during the forward sweep, and instead follows a linear rise that remains on the same the linear trend seen for $\Delta V > V_L$. This suggests that the quadratic drop in γ seen in the forward sweep does not arise from purely electrocapillarity effects ($\Delta \gamma_{EC} = -\frac{C}{2}\Delta V^2$) because those would not display any hysteresis.

2.2. Electrochemical Impedance Spectroscopy on Sessile Droplets

Using the same sessile droplet apparatus, again with 100 µL EGaIn droplets in a 1M NaOH solution, we additionally performed electrochemical impedance spectroscopy (EIS) measurements[26] and compared these results to the $\gamma(\Delta V)$ and $J(\Delta V)$ measurements presented above. All EIS experiments were performed with a constant DC bias (ΔV) superimposed with an AC voltage of amplitude 5 mV at frequencies ranging from 100 mHz to 100 MHz; the DC bias was varied from 0 to 0.5 V, corresponding to the range of the forward/backward cyclic voltammetry sweeps. Each DC bias was run six times, three times from high to low frequency (H2L), and three times from low to high frequency (L2H); the average of all six runs is plotted in **Figure 4**, and the error bars are the standard deviation among the runs. We further note that the data for the two frequency sweep directions match each other within the level of fluctuations seen within individual sweeps, validating these measurements. The EIS data was verified using the Kramer-Kronig test, as shown in the Supporting Information, and details of the Experimental Section are given in Section 4.

2.3. Interpretation of Regimes

Using the EIS data of the droplet at each ΔV, combined with observed transitions in $\gamma(\Delta V)$ and $J(\Delta V)$, we construct physical interpretations of the regimes marked by colored bands in Figures 2 and 3. At low current and voltage, the system is non-oxidizing. This regime is not the focus of our paper, but appears in our plots wherever $J < 0$ mAmm⁻². Here, the surface of the EGaIn is being reduced rather than oxidized, since $J \leqslant 0$ when $\Delta V \leqslant V_{OC}$. This observation is what allows us to reference all of our data to V_{OC}, and define $V_{OC} \equiv 0$ V.

During the lowest voltages of our forward sweeps (0 V $< \Delta V < V_P \approx 0.1$ V), J is positive and increases monotonically with ΔV (see Figure 2b). As we increase the applied potential above the open circuit potential, the surface of the droplet becomes oxidizing and we give this name to the regime shown in purple. In the Nyquist plot shown in Figure 4a,b, we observe that Re(Z) decreases compared to the values measured at $\Delta V = 0$. This indicates a decrease in charge transfer resistance, and causes the electrical current density J to increase as shown in Figure 2b. In addition, this is a charged interface, and exhibits a capacitance (or psuedocapacitance). Within this regime, γ is approximately constant (see the initial flat region in Figure 2a): if the surface contains any ions (as suggested by the impedance data), they are
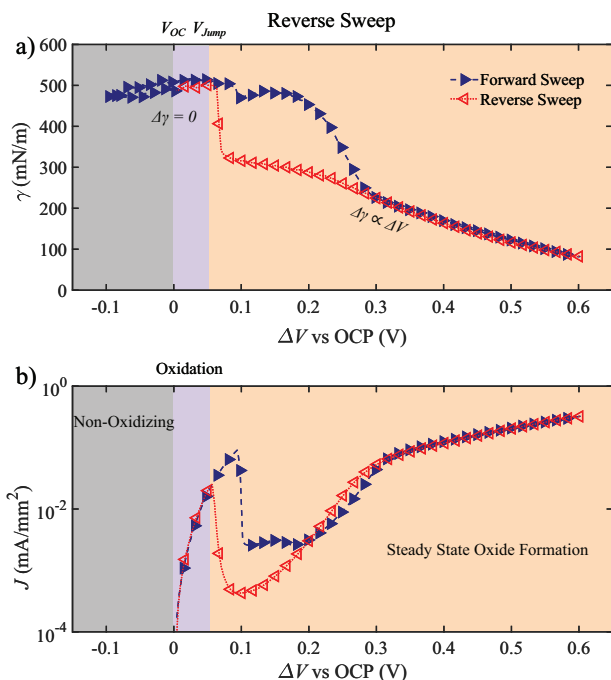

Figure 3. Typical hysteresis experiment (10 mVs⁻¹ sweep rate), with voltage shown relative to the open circuit potential V_{OC} and $\Delta V_{max} = 0.6$ V. Forward (voltage increasing) sweep is plotted as dark blue right-facing triangles, and the reverse (voltage decreasing) sweep as red left-facing triangles. Voltage-dependence of the (a) interfacial tension γ and (b) current density J are shown in parallel, with only three of the electrochemical regimes observed — non-oxidizing, oxidation, and steady state oxide formation — as defined by the behavior of γ and J in the reverse sweep. The transpassive regime is not observed on the reverse sweep. Note that the purple curves are repeated from Figure 2.

**ADVANCED
SCIENCE NEWS**
www.advancedsciencenews.com

**ADVANCED
FUNCTIONAL
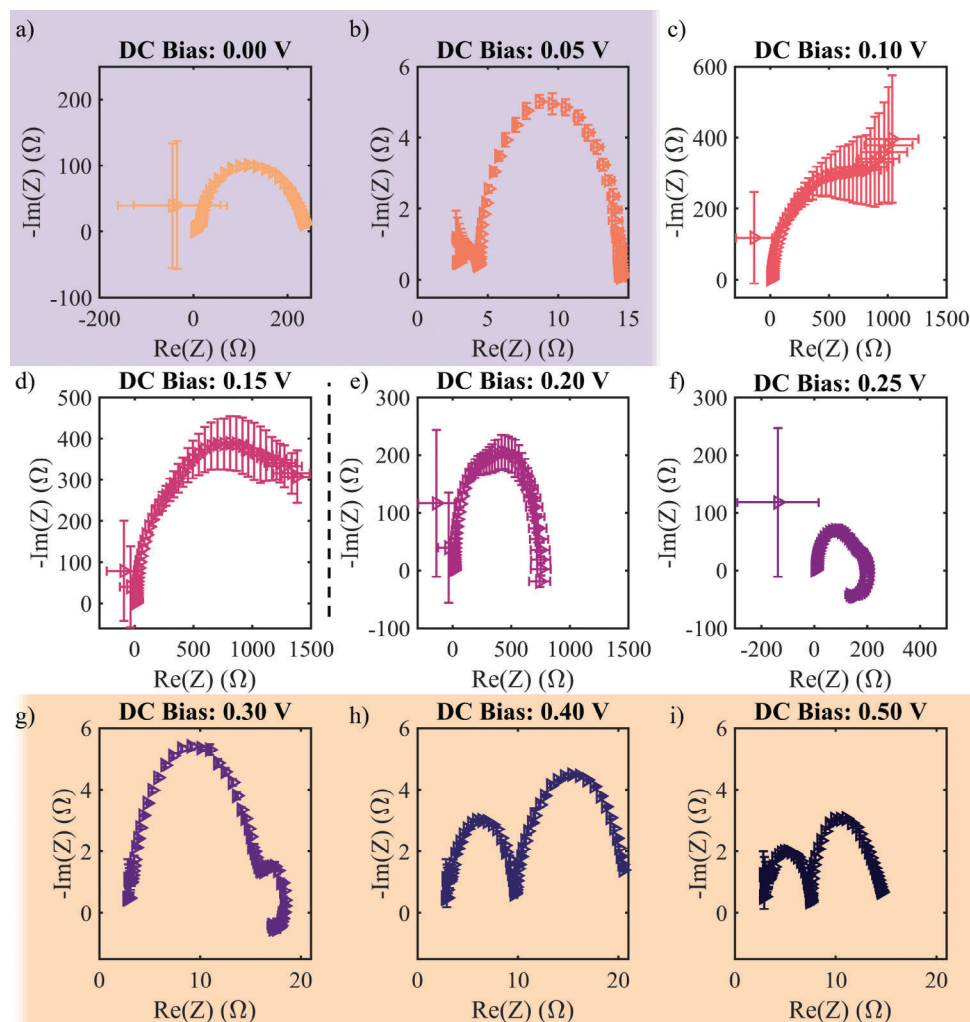MATERIALS**
www.afm-journal.de

Figure 4. Nyquist diagrams of the electrochemical impedance spectroscopy at various DC biases during a forward potential sweep; each data point at a specific DC bias is the average of all six runs (both H2L and L2H) and the error bars are the standard deviation among them. a,b) Low voltage oxidation regime, with purple background. c–f) Medium voltage transpassive regime, with white background (g–i) High voltage steady state oxide formation regime, with orange background. Background colors correspond to those used in Figure 2, and the dashed line between (d) and (e) corresponds to the same line drawn in Figure 3, the transition between diffusive and inductive transpassive behavior.

not surface-active. In addition, the dissolution rate of the gallium oxide species is at least as large as the oxidation rate.

This regime ends for $V > V_P$, at which point J drops by two orders of magnitude (see Figure 2b). We interpret this as the minimum voltage at which the oxidized gallium species first coats the entire surface of the droplet, creating a passivating layer that strongly suppresses additional electrochemical reactions. We call this regime above V_P the transpassive regime, as it occurs after the breakdown of passivation.

Within this regime (between V_P and V_{SQ}), we observed small changes in J depending on the extent to which the NaOH solution was reused, but there were no changes in γ observed when using fresh 1M NaOH. The reuse of solution presumably creates conditions in which the concentration of dissolved gallium becomes large enough to cause a dip in γ around V_P. Fortuitously, these experiments allow us to conclude that the oxidation species must not be changing the chemical potential of the Ga–NaOH$_{aq}$ inter-

face enough to observe the change until the concentration of Ga dissolved in NaOH$_{aq}$ becomes significant. Therefore, we believe the oxidation species is an adsorbed gallium hydroxide such that the total number of gallium atoms and hydroxide ions at the interface does not change above and below V_P. Gallium oxide dissolves into Ga(OH)$_4^-$, which is stable in its dissolved form in NaOH,[27] and therefore the concentration of Ga(OH)$_4^-$ in the NaOH solution increases with each run of the experiment. Once the concentration of Ga(OH)$_4^-$ is high enough, the dip in γ at $\Delta V \approx V_P$ appears in our data. This hypothesis is supported by the Nyquist plots: the impedance data decays into a linear tail, which implies the interface is diffusive.[28,29] Future direct measurements of ion concentration (e.g., Ga^{3+}) would allow for testing the validity of these interpretations.

Interestingly, we observe a small local maximum in both γ and J near the middle (0.15 V, dashed vertical line) of the transpassive regime, which indicates that the oxide species on the surface

**ADVANCED
SCIENCE NEWS**

www.advancedsciencenews.com

**ADVANCED
FUNCTIONAL
MATERIALS**

www.afm-journal.de

of the metal changes to a different species in the vicinity of this potential.[30] This is a much smaller effect than the initial oxidation peak in J that delineates the oxidation regime. The large oxidation peak likely corresponds to the adsorption of gallium hydroxides, while this secondary transpassive peak arises from the formation of gallium oxide, either Ga_2O_3 or $GaOOH$ according to the literature.[31] As the system moves into this transpassive regime, the composition of the oxide film starts to change; this can be identified by the Nyquist plots changing from diffusive (Figure 4c,d) to inductive (panels e,f). This also coincides with changes in the interfacial tension (see Figure 2). Such a change in oxide has been observed in anodic dissolution of mild steel, suggesting presence of an adsorbed layer of FeOH associated with transpassivation.[32]

From the secondary transpassive peak onward to higher ΔV, marked by a dashed black line in the Figure 2, we observed that γ decreases quadratically (proportional to ΔV^2). If this oxide layer has approximately constant capacitance in this subregime (as will be measured in Section 2.4), then the energy density of the surface layer (Jm^{-2}, equivalent to interfacial tension Nm^{-1}) due to the resulting charge separation would be proportional to ΔV^2, as is observed here. Note, however, that this γ-dependence only appears during the forward sweep, and not the reverse sweep. This suggests that any capacitive charge separation is not reversible, and is perhaps only metastable. As will be discussed in Section 2.4, this explanation is preferred over electrocapillary explanations due to the anomalously large values of the capacitance observed.

Care is required when interpreting the Nyquist plots within the quadratic subregime ($V_{SQ} < \Delta V < V_L$) due to a few caveats. Within our data, we observe an increase in both the real and imaginary components of the impedance for sequential runs, a phenomenon known as drift. This arises from changes to the surface of the working electrode that are irreversible within the timescale between runs of the experiment.[33] Since we believe that the interface transitions from gallium hydroxide to gallium oxide within this regime, such drift is to be expected. We also observe an induction loop that crosses the $Im(Z) = 0$ line, which is likely due to the droplet physically oscillating, generating new surface area during the frequency sweep.

Finally, above V_L, the system switches multiple behaviors all at the same voltage: J becomes an exponential function of ΔV, γ decreases linearly with ΔV, and the Nyquist plots show a transition from having a single semicircle with an induction loop that crosses $Im(Z) = 0\,\Omega$ to having two semicircles with $Im(Z) < 0$ for all frequencies measured. We interpret the J-dependence as arising from new reactions at the metal-oxide interface, in which ions are driven through the surface layer;[34] we call this the steady state oxide formation regime. In this interpretation, at $\Delta V = V_L$, the surface concentration Γ_{ox} has reached its maximum concentration for a single layer, and any new oxide now must form multiple layers. Such behavior is consistent with what has been observed for aluminum in its steady state oxide formation regime: that the amount of oxide shell material is proportional to the applied anodization potential,[35] and that the decrease in γ is due to stress in the oxide layer induced by ΔV.[36] The Nyquist plots in this regime (see Figure 4g–i) all show two semicircles, an observation consistent with the system having two timescales as is typically seen for coatings of metals. We further observe that experiments in this regime are highly reproducible, as the oxide is likely too stiff to support the oscillations that interfered with measurements at lower voltages.

As shown in Figure 3, only three of the four regimes are present during a reverse sweep due to hysteresis. There is no longer a quadratic subregime, and the two branches re-merge only for $V_{jump} < V_{SQ}$. The hysteresis implies that the oxide layer remains thick enough for the mechanisms of the steady state oxide formation regime to remain dominant, possibly because the gallium oxide shell is insoluble within the timescale of these experiments. This would mean the surface species do not revert during the reverse sweep, and instead maintain the behavior observed in the steady state oxide regime.

To test this hypothesis, we ran additional hysteresis experiments with different values of V_{max}, spanning both the transpassive and steady state oxide formation regimes. The results are shown in **Figure 5**. We observed that if $V_{max} > V_L$, then the hysteresis curve remains as presented above, while for $V_{max} < V_L$ the hysteretic effects are reduced. In these less-hysteretic experiments, γ remained constant upon reversal, again jumping back to the original branch at $\Delta V = V_{jump}$. This confirms that gallium oxide is likely insoluble for $\Delta V > V_{jump}$ within the timescale of these experiments. Notably, when $\Delta V < V_{jump}$ the droplet maintains γ_0, likely due to the oxidation rate of the EGaIn dropping below the dissolution rate of the gallium oxide, after which the oxide is quickly removed from the surface. This is visible in Figure 5. Since gallium oxide reduces the amount of hydroxide (OH^- or $Ga(OH)_4^-$) on the interface of the metal, it reduces the chemical potential between the bulk EGaIn and the metal-electrolyte interface. This creates a decrease in the surface energy density, which is proportional to the oxide concentration.

We summarize all of the above, schematically, in **Figure 6**. During the forward sweep (increasing voltage, panel a), the EGaIn is bare from V_{OC} to V_P, at which point the surface begins to be covered with adsorbed gallium hydroxide. From V_{SQ} to V_L, the surface coverage transitions to being gallium oxide, with $\Delta\gamma \propto \Delta V^2$ an approximately constant capacitance across an oxide layer of approximately constant thickness (a monomolecular layer). Beyond V_L, this oxide shell may become thicker, but such measurements are beyond the scope of this paper. In any case, $\Delta\gamma$ is now mainly arising due to a voltage induced stress in the oxide layer. During the reverse sweep (decreasing voltage, panel b), the oxide layer is gradually dissolved as the dissolution rate increases relative to the oxidation rate. At timescales longer than these experiments, this transient state might be eliminated if the sweep were slow enough. At V_{jump} the dissolution rate exceeds the oxidation rate by a large enough amount that the system returns to its original, bare state.

2.4. Modeling

Using our oxidation cartoon, we can create equivalent circuits (see **Figure 7**) for the different electrochemical regimes, and then use these to fit the Nyquist plots using the capacitance and resistance values as fit parameters. All circuits start with the resistance of the electrolyte solution R_{sol}, in series with additional effects associated to the particular regime.
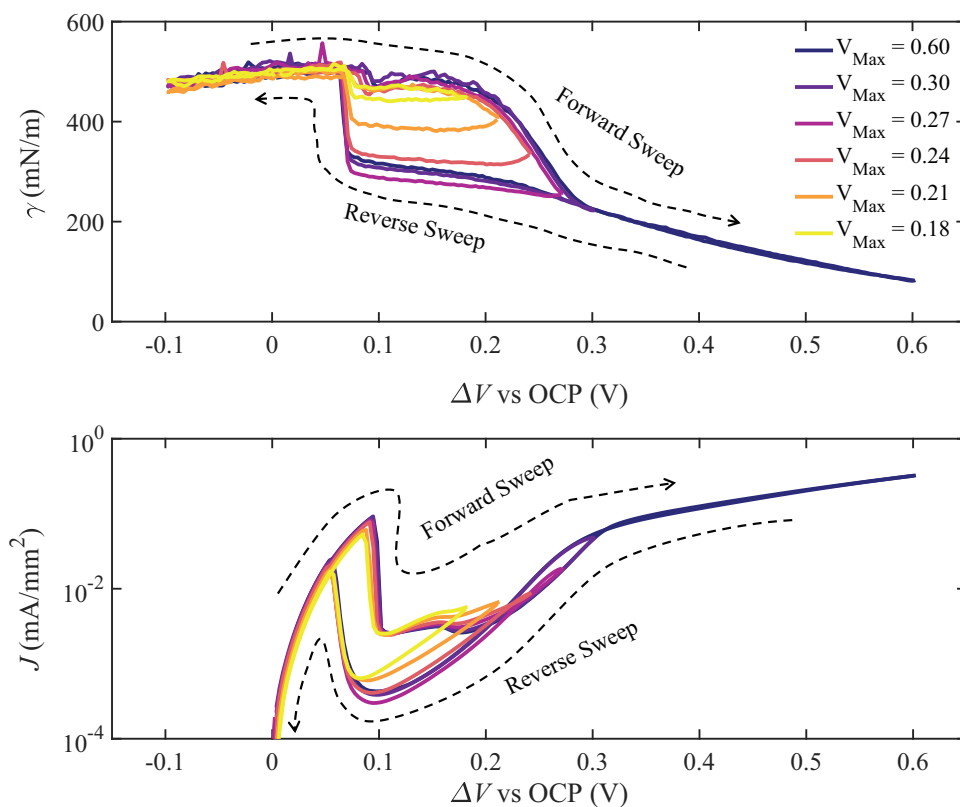
**ADVANCED
SCIENCE NEWS**

www.advancedsciencenews.com

**ADVANCED
FUNCTIONAL
MATERIALS**

www.afm-journal.de

Figure 5. The observed hysteresis at a 10 mVs^{-1} sweep rate with various maximum voltages. Dark purple curves are at higher V_{max}; light yellow curves are at lower V_{max}. The hysteretic transition is again visible (as in Figure 3) at $\Delta V_{jump} \approx 0.06$ V; the curve for $\Delta V_{max} = 0.6$ V is the same dataset.
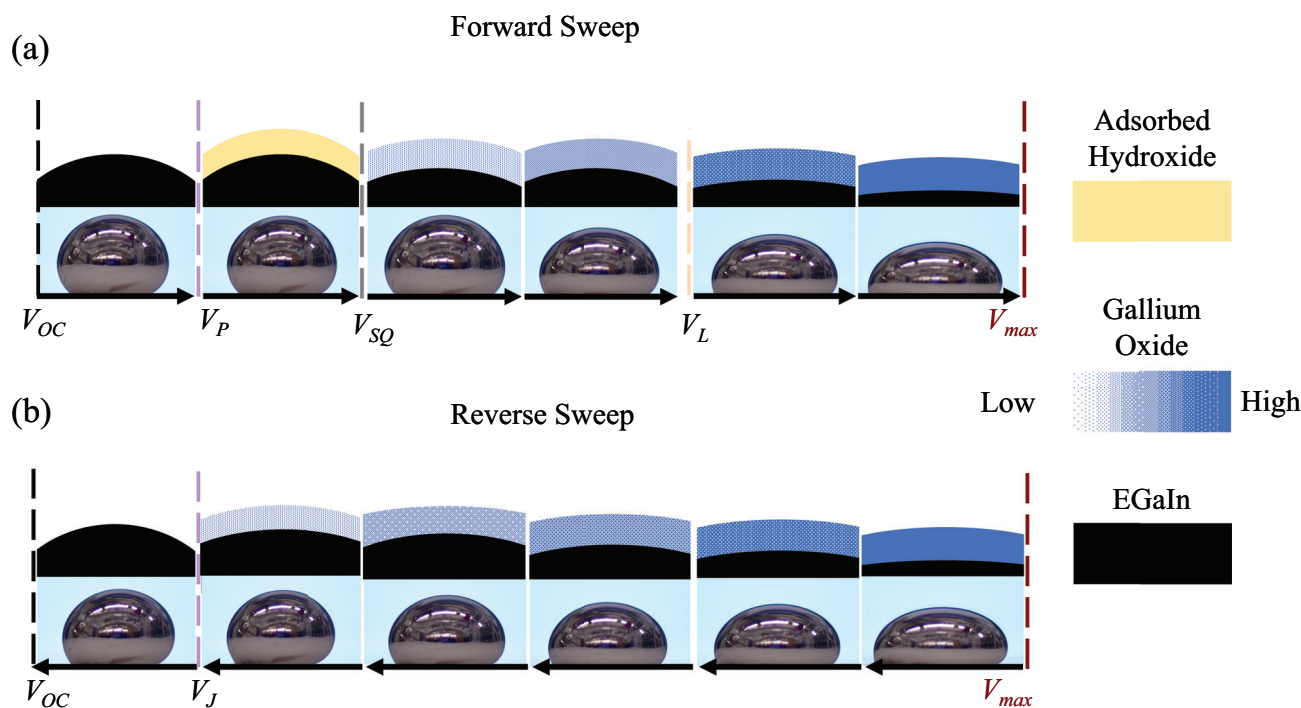

Figure 6. Cartoon of the proposed surface oxidation responsible for lowering the interfacial tension. Each EGaIn droplet is shown bare, with a light yellow layer representing adsorbed gallium hydroxide, or with a blue layer of changing Γ (can either change due to surface density or oxide thickness).

ADVANCED
SCIENCE NEWS

www.advancedsciencenews.com
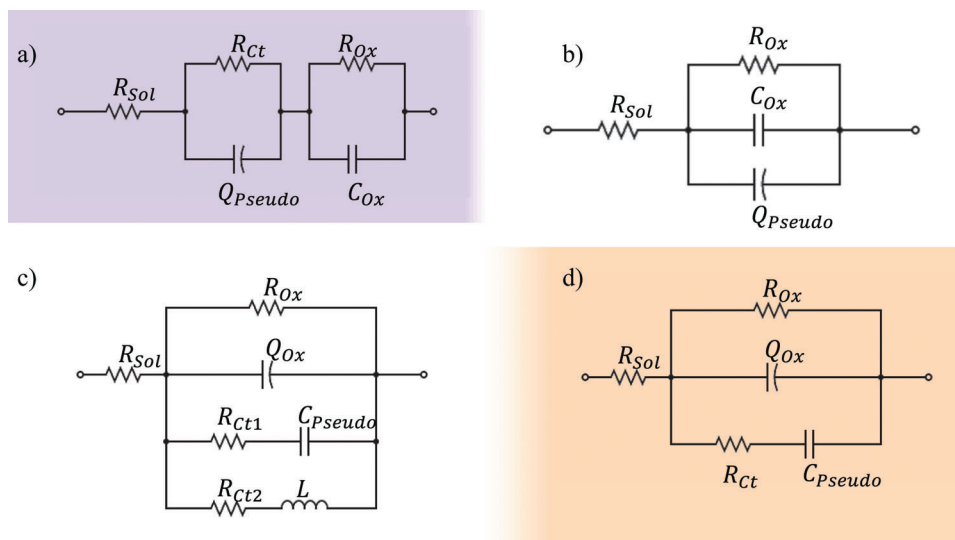
ADVANCED
FUNCTIONAL
MATERIALS

www.afm-journal.de

Figure 7. Equivalent circuits for the a) oxidation, b) early transpassive (diffusive), c) late transpassive (inductive), and d) steady state oxide formation regimes. Colors correspond to regimes marked in Figure 2.

For the oxidation regime (purple, see panel a), we first include a circuit element to model the charge transfer resistance R_{ct}, and a non-ideal pseudocapacitance Q_{pseudo}; these describe the chemical reactions occurring at the interface, in parallel with each other. Second, there's an additional element with both the oxide resistance R_{ox} and capacitance, C_{ox}, which describe the oxide itself.

For the transpassive regime (white, see panels b and c), we include several elements in parallel: the resistance R_{ox} and capacitence C_{ox} of the oxide layer, also in parallel with a pseudocapacitance Q_{pseudo} describing the reaction of a the species diffusing through and around the shell. Once the voltage is above V_{SQ}, it is necessary to adjust this circuit to account for the inductive behavior we see in the Nyquist plots. We have modeled these effects by making the oxide instead have a pseudocapacitance Q_{ox}, and then adding two parallel charge transfer paths, one describing the reaction with an ideal pseudocapacitance C_{pseudo} in series with a charge transfer resistance R_{Ct1}, and one describing the electrical

induction L, caused by the changing area of the droplet in series with a charge transfer resistance R_{Ct2}.

For the steady state oxide formation regime (orange, see panel d), we remove the inductive behavior and place several elements in parallel: the resistance R_{ox} and pseudocapacitence Q_{ox} of the oxide layer remain as before, but the additional charge transfer path is a charge transfer resistance R_{ct} in series with C_{pseudo}, to model ions pushing through the oxide layer to reach the pure gallium interface.

Figure 8 evaluates the results of these simplified models when fitting data such as that shown in Figure 4. Panel a shows how C_{ox} and C_{pseudo} change with increasing applied voltage. The oxide capacitance initially grows during the oxidation regime, then drops and remains below $20\,\mu Fcm^{-2}$ for higher voltages, while the pseudocapacitance remains around or below $100\,\mu Fcm^{-2}$ until the steady state oxide formation regime where it grows to over $1000\,\mu Fcm^{-2}$. The resistance fits are shown in panel b: the
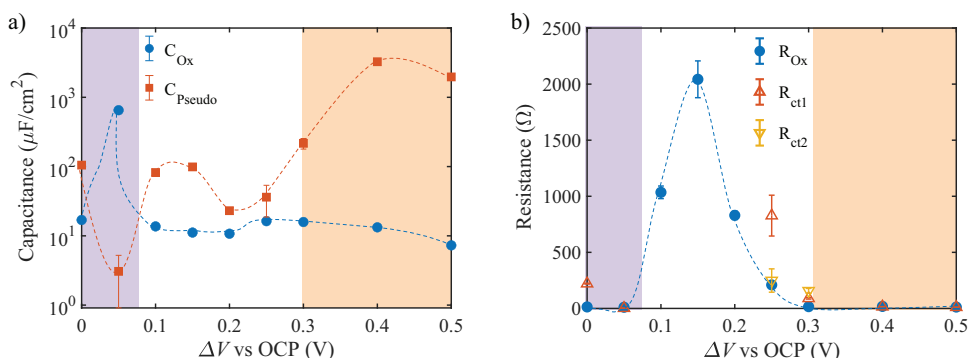

Figure 8. Parameters obtained by fitting the L2H Nyquist plots to equivalent circuit models (Figure 7) using a non-linear least square fit. Example fits are shown in the Supplemental Material. a) Capacitance (blue cirlces) and pseudocapacitance (orange squares) and b) oxide resistance (blue circles) and two charge transfer resistances (orange and yellow triangles). Dashed lines are to guide the eye and colored bands correspond to the regimes marked in Figure 2.

2311501 (7 of 10)

**ADVANCED
SCIENCE NEWS**

www.advancedsciencenews.com

**ADVANCED
FUNCTIONAL
MATERIALS**

www.afm-journal.de

resistance grows until a maximum near V_{SQ}, after which it drops again.

These effective circuit parameters also permit a comparison to some idealized models for the interfacial tension, assuming that all capacitive elements store energy at the interface, and therefore correspond to surface energies.[37] In the quadratic subregime within the transpassive, we observe $\Delta\gamma(\Delta V)\propto\Delta V^2$. If this were due solely to electrocapillarity effects, we would expect $\Delta\gamma(\Delta V) = C_{EC}\Delta V^2$.[38] For the observed changes in γ, this would require $C_{EC} = (3200 \pm 50)\,\mu Fcm^{-2}$. As this value is an order of magnitude larger than the values of C_{ox} we found by fitting the Nyquist plots in this regime (see Figure 8a), it is unlikely that the observed decrease in γ can be accounted for solely by traditional electrocapillarity. Note that this value of C_{EC} is also an order of magnitude larger than C_{pseudo} measured in the same regime, but is on the same order as C_{pseudo} measured in the steady state oxide formation regime.

We can understand the linear γ regime (above V_L for the forward sweep, above V_{jump} for the backward sweep) in terms of the Gibbs adsorption isotherm equation. We consider $\Delta\gamma = -\sum N_{ox}/a\Delta\mu_{ox}$,[39] where N_{ox}/a is the concentration of gallium oxide on the interface and $\Delta\mu_{ox}$ is the difference in chemical potential between gallium oxide and pure gallium in 1M NaOH. While the values for $N_{ox}(\Delta V)$ and $\Delta\mu_{ox}$ are not measured here, we can assume $\Delta N_{ox}\propto\Delta V$. Starting from an initially-bare metal interface, we integrate to find $N(\Delta V) = \frac{dN}{dV}\Delta V$, which predicts a functional form

$$\Delta\gamma(\Delta V) = \frac{\Delta\mu_{ox}}{a}\frac{dN}{dV}\Delta V \qquad (1)$$

for which we measure the prefactor to be $\frac{\Delta\mu_{ox}}{a}\frac{dN}{dV} = (59 \pm 4)\frac{nmol}{V\,cm^2}\frac{kJ}{mol}$. Unfortunately we do not have enough information to determine whether N_{ox}/a is changing by increasing the surface concentraion of the oxide, or by increasing the thickness of the oxide layer. If we did, we could use this value to estimate the relative permittivity of the oxide layer, which would help us determine the oxide species. Or if we knew the oxide species, we could determine if the oxide was growing in surface density or in thickness during this regime and we could compare this what we learned from the Nyquist plots.

These models also allow us to understand some of the results presented in Figure 4a-b, where the data are consistent with a decrease in charge transfer resistance R_{ct} in two voltage ranges: both from 0 and 0.0.5 V and also above 0.3 V. These are also the same two regimes for which holding the potential steady produces a steady state current that does not decay to zero. This implies that the oxide species that form on the surface due to electrochemical oxidation dissolve, and therefore do not accumulate on the surface beyond a steady state thickness. Such behavior is consistent with low charge transfer resistance. In the regime between 0.1 to 0.25 V, the current is very low due to passivation and thus, we do not report R_{ct} values in this range since resistance at the surface is dominated by the oxide (R_{Ox}). Ongoing work in our laboratory suggests that the passivating species between ≈ 0.1 to 0.3 V may be GaOOH. In contrast, soluble species (gallate salts) form beyond the passivation regime (steady state oxide formation).

3. Conclusion

During this investigation into the dependence of the interfacial tension γ on the applied electric potential ΔV, we observed that γ can be reproducibly tuned for $\Delta V > V_L$, but for $V_P < \Delta V < V_L$ γ depends on the history of the droplet, as shown in Figure 5. It is apparent that during the forward sweep (increasing ΔV from the open circuit potential to a more positive potential), there are three different behaviors of γ: γ independent of ΔV, γ decreasing proportional to ΔV^2, and γ decreasing linearly with ΔV. A small regime with a fourth behavior — a small dip in γ at $\Delta V \approx V_P$ — occurs only if the electrolyte solution is polluted with $Ga(OH)_4^-$.

We have found that the regime where $\Delta\gamma\propto\Delta V^2$, the decrease in γ is not likely due to electrocapillarity as (1) the capacitance required for this regime to be electrocapillarity is too large, and (2) electrocapillarity should not show hysteresis. It is also likely not due to a voltage-induced tangential stress in the oxide as changing the sweep direction below V_L leads to a $\Delta\gamma \approx 0$. The $\Delta\gamma\propto\Delta V^2$ behavior occurs for values of ΔV beyond the second oxidation peak, and is therefore most likely due to the change in chemical potential of the interface due to the formation of an insoluble gallium oxide, either Ga_2O_3 or GaOOH. Future research could address making quantitative predictions for the prefactor, based on propoerties of the oxides present. The regime where γ decreases linearly with ΔV can be attributed to a voltage-induced tangential stress in the gallium oxide layer. In the reverse sweep, γ increased linearly with decreasing ΔV for $\Delta V > V_{jump}$, since the gallium oxide layers in insoluble at these potentials in the timescale of these experiments. Finally, γ returns to the bare metal value for $\Delta V < V_{jump}$, which appears to be due the oxidation rate of the EGaIn being much less than the dissolution rate of the oxide, which leads to the droplet reverting back to a bare metal at these electric potentials.

We have presented several studies which, when taken together, increase our understanding of possible mechanisms for the drop in interfacial tension with applied voltage. The hysteresis reported here has, to our knowledge, not previously been reported. The decrease in γ for all oxidation potentials has previously been assumed to be due to the concentration of gallium oxide on the surface of the metal. Once the exact molecular forms of the gallium hydroxides and gallium oxide are known, the surface concentrations can be determined as a function of ΔV, it will be possible to build a free energy model of γ as a function of ΔV. However, directly observing the oxide at these electric potentials is difficult as all forms of gallium oxide are optically transparent, and so directly measuring the concentration of the oxide in this voltage range has proven a challenge. Measuring the rheology of anodizing EGaIn in 1M NaOH may help to better understand the mechanisms involved in the behavior of $\gamma(\Delta V)$, allowing the chemical and interfacial mechanisms to be distinguished.

4. Experimental Section

Sessile Drop Technique: The sessile drop technique was a technique in which a sessile (immobile) droplet was imaged from the side so that the shape of the droplet on a substrate could be directly measured. There were various ways the interfacial tension could be extracted from the image, from the one-component Zisman theory,[40] the two-component Owens/Wendt theory,[41] to the three-component van Oss theory.[42] For

this work, it used calculations derived by Hutzler et al.:[43] these were an application of Morse-Witten theory to sessile and pendant drops under a small force, originally derived to model the deformation of a droplet in an emulsion.[44] It was valid for large values of γ, as it had here, and the approximation was based on both the maximum equatorial drop radius L_x, and the distance from the equator to the top of the droplet L_z. As such, a key benefit was that it did not require measuring the contact angle between the EGaIn and the acrylic substrate; this was particularly important because droplets sometimes become pinned at their base.

For a sessile droplet, γ is calculated using the following equation:

$$\gamma(L_z, L_x) \approx \Delta\rho g \frac{\ln(2)}{24} \frac{(L_z + L_x)^3}{|L_z - L_x|} (1 - 3c + 3c^2 - c^3) \tag{2}$$

where the constant $c = \frac{1 - \ln(2)}{\ln(2)} \frac{|L_z - L_x|}{L_z + L_x}$ is a correction due to the difference in the derived formula and the values measured by Hutzler et al.[43] A needle with an outer diameter of 1.26 mm was placed in the photos, directly above the droplet, as a reference to determine the number of pixels per mm. It calculated the area a of the droplet using edge detection. Assuming radial symmetry, a is calculated by rotating the edges around the z-axis, $a = \sum_i \pi(\frac{|x_{i+1} + x_i|}{2})\Delta s_i$, where x_i and y_i are the positions of the edge pixels, and $\Delta s_i^2 = \Delta x_i^2 + \Delta y_i^2$. A sample analysis is shown in the Figure S2 (Supporting Information).

Cyclic Voltammetry: To oxidize the liquid metal, it used a three electrode setup consisting of a working electrode, a counter electrode, and a reference electrode as shown in Figure 1. For the majority of the experiments, it used a Biologic potentiostat; the EGaIn droplet acted as the working electrode. A thin copper wire, which was connected to the power supply, was pushed through the bottom of an acrylic substrate, and a 100 µL of EGaIn was wet to the wire. The substrate was leveled so that the droplet would remain in place and in electrical contact with the wire during the course of the experiment. A platinum mesh electrode was used for the counter electrode and was placed on the edge of the NaOH bath to minimize gradients in the electric field at the surface of the droplet. The Ag/AgCl/KCl reference electrode (2M KCl) was placed as close to the EGaIn as possible without touching the droplet at its widest spreading and being far enough away as not to interfere with the imaging of the droplet.

It tested several different sweep rates: 1, 10, 50, 100, and 300 mVs^{-1}, all from −1.63 to −0.93 V, to determine the maximum sweep rate for which the droplet dynamics were significantly faster than the chemical reaction rates, so that the droplet remains near steady-state. The fastest of these sweep rates (300 mVs^{-1}) caused the droplet shape to change so quickly that it was difficult to obtain an accurate measurement of γ. At 1 mVs^{-1} it was not possible to complete a full cycle during the Nikon D850's camera's available recording duration. Therefore, it selected 10 mVs^{-1} as the sweep rate, which was slow enough for the droplet dynamics to remain near steady-state. Sample data for a variety of sweep rates was shown in the Supporting Information.

To compare the results of this experiment with other experiments of different shapes and sizes, I was converted to current density J by dividing out the exposed (upper) surface area a of the droplet: $J = I/a$. At the base of the droplet, $J \approx 0$ mAmm^{-2} for the surface of the droplet in contact with the substrate, so it did not contribute to the current density.

Electrochemical Impedance Spectroscopy: The EIS experiments used the same sessile drop design as the cyclic voltammetry experiments. A copper wire was connected to a 100 µL EGaIn droplet, a platinum mesh was used for the counter electrode, and an Ag/AgCl/KCl electrode was used for the reference electrode. The experiment was performed in a 1M NaOH bath using the Biologic potentiostat. The EIS experiments were held at a constant DC bias with a 5 mV AC amplitude, applied from 100 mHz to 100 MHz with 12 points per decade. It observed that for a larger AC amplitude (10 mV), the results were less reproducible than at 5 mV.

Supporting Information

Supporting Information is available from the Wiley Online Library or from the author.

Conflict of Interest

The authors declare no conflict of interest.

Data Availability Statement

The data that support the findings of this study are openly available in DataDryad at https://doi.org/10.5061/dryad.2z34tmpsb.

[1] A. Dey, R. Guldiken, G. Mumcu, *IEEE Trans. Antennas Propag.* **2016**, *64*, 2572.

[2] C. B. Eaker, I. D. Joshipura, L. R. Maxwell, J. Heikenfeld, M. D. Dickey, *Lab Chip* **2017**, *17*, 1069.

[3] M. R. Khan, C. B. Eaker, E. F. Bowden, M. D. Dickey, *Proc. Natl. Acad. Sci.* **2014**, *111*, 14047.

[4] I. D. Joshipura, M. Finn, S. T. M. Tan, M. D. Dickey, D. J. Lipomi, *MRS Bull.* **2017**, *42*, 960.

[5] S. Chen, L. Wang, Q. Zhang, J. Liu, *Sci. Bull.* **2018**, *63*, 1513.

[6] V. Vallem, Y. Sargolzaeiaval, M. Ozturk, Y.-C. Lai, M. D. Dickey, *Adv. Mater.* **2021**, *33*, 2004832.

[7] Y. Wang, J. Guo, Y. Fang, G. Pang, J. Wang, X. Wang, C. Jiao, X. Chen, K. Sun, L. Hu, *Adv. Mater. Interfaces* **2021**, *8*, 2100954.

[8] S.-Y. Tang, K. Khoshmanesh, V. Sivan, P. Petersen, A. P. O'Mullane, D. Abbott, A. Mitchell, K. Kalantar-zadeh, *Proc. Natl. Acad. Sci.* **2014**, *111*, 3304.

[9] Z. Yu, Y. Chen, F. F. Yun, D. Cortie, L. Jiang, X. Wang, *Phys. Rev. Lett.* **2018**, *121*, 024302.

[10] M. L. Berre, Y. Chen, C. Crozatier, Z. Zhang, *Microelectron. Eng.* **2005**, *78–79*, 93.

[11] R. C. Gough, A. M. Morishita, J. H. Dang, W. Hu, W. A. Shiroma, A. T. Ohta, *IEEE Access* **2014**, *2*, 874.

[12] K. Khoshmanesh, S.-Y. Tang, J. Y. Zhu, S. Schaefer, A. Mitchell, K. Kalantar-zadeh, M. D. Dickey, *Lab Chip* **2017**, *17*, 974.

[13] H.-J. Kim, C. Son, B. Ziaie, *Appl. Phys. Lett.* **2008**, *92*, 011904.

[14] M. D. Dickey, R. C. Chiechi, R. J. Larsen, E. A. Weiss, D. A. Weitz, G. M. Whitesides, *Adv. Funct. Mater.* **2008**, *18*, 1097.

[15] M. R. Khan, C. Trlica, M. D. Dickey, *Adv. Funct. Mater.* **2015**, *25*, 671.

[16] T. Jung, S. Yang, *Sensors* **2015**, *15*, 11823.

**ADVANCED
SCIENCE NEWS**

www.advancedsciencenews.com

**ADVANCED
FUNCTIONAL
MATERIALS**

www.afm-journal.de

[17] H. B. de Aguiar, A. G. F. de Beer, M. L. Strader, S. Roke, *J. Am. Chem. Soc.* **2010**, *132*, 2122.

[18] Y. Liu, P. G. Jessop, M. Cunningham, C. A. Eckert, C. L. Liotta, *Science* **2006**, *313*, 958.

[19] R. C. Gough, A. M. Morishita, J. H. Dang, M. R. Moorefield, W. A. Shiroma, A. T. Ohta, *Micro and Nano Syst. Lett.* **2015**, *3*, 4.

[20] D. J. C. M. 't Mannetje, F. Mugele, D. van den Ende, *Langmuir* **2013**, *29*, 15116.

[21] G. Cha, C.-J. Kim, Y. S. Ju, *Appl. Therm. Eng.* **2016**, *98*, 189.

[22] C. B. Eaker, D. C. Hight, J. D. O'Regan, M. D. Dickey, K. E. Daniels, *Phys. Rev. Lett.* **2017**, *119*, 17.

[23] M. Song, K. Kartawira, K. D. Hillaire, C. Li, C. B. Eaker, A. Kiani, K. E. Daniels, M. D. Dickey, *Proc. Natl. Acad. Sci.* **2020**, *117*, 19026.

[24] Y. He, J. Tang, K. Kalantar-Zadeh, M. D. Dickey, X. Wang, *Proc. Natl. Acad. Sci.* **2022**, *119*, e2117535119.

[25] A. E. Gheribi, P. Chartrand, *Sci. Rep.* **2019**, *9*, 7113.

[26] V. Vivier, M. E. Orazem, *Chem. Rev.* **2022**, *122*, 11131.

[27] I. I. Diakonov, G. S. Pokrovski, P. Bénézeth, J. Schott, J.-L. Dandurand, J. Escalier, *Geochim. Cosmochim. Acta* **1997**, *61*, 1333.

[28] D. Pletcher, R. Greff, R. Peat, L. M. Peter, J. Robinson, *Instrumental methods in electrochemistry*, Woodhead Publishing, Cambridge [England], **2011**, oCLC: 874155972.

[29] M. E. Orazem, B. Tribollet, *Electrochemical Impedance Spectroscopy: Orazem/Electrochemical*, John Wiley & Sons, Inc., Hoboken, NJ, USA, **2008**.

[30] A. J. Bard, L. R. Faulkner, *Electrochemical Methods: Fundamentals and Applications*, 2nd ed. edition, Wiley, New York **2001**.

[31] Y. Chung, C.-W. Lee, *J. Electrochem. Sci. Technol.* **2013**, *4*, 1.

[32] P. Li, T. C. Tan, J. Y. Lee, *Corros. Sci.* **1996**, *38*, 1935.

[33] E. Ziino, S. Marnoto, J. M. Halpern, *ECS Trans.* **2020**, *97*, 737.

[34] D. D. Macdonald, S. Real, S. I. Smedley, M. Urquidi-Macdonald, *J. Electrochem. Soc.* **1988**, *135*, 2410.

[35] M. Mibus, C. Jensen, X. Hu, C. Knospe, M. L. Reed, G. Zangari, *J. Appl. Phys.* **2013**, *114*, 014901.

[36] W. Haiss, *Rep. Prog. Phys.* **2001**, *64*, 591.

[37] K. Hillaire, PhD, North Carolina State University, Raleigh, NC, **2022**.

[38] D. C. Grahame, *Chem. Rev.* **1947**, *41*, 441.

[39] H.-J. Butt, K. Graf, M. Kappl, *Physics and Chemistry of Interfaces*, Physics Textbook, Wiley-VCH, Weinheim, **2003**.

[40] (Ed.: F. M. Fowkes), *Contact Angle, Wettability, and Adhesion, of Advances in Chemistry*, vol. *43*, American Chemical Society, Washington, D.C. **1964**.

[41] D. K. Owens, R. C. Wendt, *J. Appl. Polym. Sci.* **1969**, *13*, 1741.

[42] R. J. Good, C. J. van Oss, in *Modern Approaches to Wettability*, (Eds.: M. E. Schrader, G. I. Loeb), Springer US, Boston, MA **1992**, pp. 1–27.

[43] S. Hutzler, J. C. F. Ryan-Purcell, F. F. Dunne, D. Weaire, *Philos. Mag. Lett.* **2018**, *98*, 9.

[44] D. C. Morse, T. A. Witten, *Europhys. Lett.* **1993**, *22*, 549.